Applied Catalysis B: Environmental 164 (2015) 31–39

Contents lists available at ScienceDirect

Applied Catalysis B: Environmental

journal homepage: www.elsevier.com/locate/apcatb

Vanadium pyrophosphate oxides: The role of preparation chemistry in determining renewable acrolein production from glycerol dehydration

Xinzhen Feng[a], Yao Yao[a], Qin Su[a], Liang Zhao[a], Wu Jiang[a], Weijie Ji[a,*], Chak-Tong Au[b]

[a] Key Laboratory of Mesoscopic Chemistry, MOE, School of Chemistry and Chemical Engineering, Nanjing University, Nanjing 210093, China
[b] Department of Chemistry, Hong Kong Baptist University, Kowloon Tong, Hong Kong

ARTICLE INFO

Article history:
Received 24 May 2014
Received in revised form 28 August 2014
Accepted 31 August 2014
Available online 6 September 2014

Keywords:
Glycerol
Dehydration
Acrolein
Vanadium pyrophosphate oxide
Preparation chemistry

ABSTRACT

Efficient acrolein production through selective dehydration of biomass-derivable glycerol was investigated over the vanadium pyrophosphate oxide (VPO) catalysts. Employing polyethylene glycol (PEG) additive in the preparation media and activating the VPO precursors in the butane–air atmosphere considerably enhanced catalyst performance for the target reaction. An acrolein yield of 70.1 mol% can be achieved over the as-synthesized VPO catalyst using an aqueous glycerol solution (36.5 wt.%) feed and a liquid hourly space velocity (LHSV) of 4 h^{-1} at 320 °C. Moreover, the derived VPO catalyst can handle heavy loading of reaction feed, such as a concentrated glycerol solution (50.0 wt%) or a notably high LHSV of 12 h^{-1}, and still retain reasonable acrolein yields (45–65 mol%), giving acrolein formation rate up to 35.3 mmol g_{cat}^{-1} h^{-1}. Techniques including X-ray diffraction (XRD), scanning electron microscopy (SEM), X-ray photoelectron spectroscopy (XPS), Raman spectroscopy, and hydrogen temperature programmed reduction (H_2-TPR) were employed to explore the nature of catalysts. Type of alcohol and addition of PEG adopted in catalyst preparation showed significant impact on sample crystallinity/morphology, surface V^{5+}/V^{4+} ratio, V—O bonding strength, and Brønsted surface acidity. Balanced surface V^{5+}/V^{4+} ratio and suitable density of medium strong acid sites are found to be critical to accomplish superior activity.

1. Introduction

As fossil resources deplete and increasing concerns about environmental issues, the utilization of biomass-derivable feedstock is of great interest [1–3]. The biomass-derivable glycerol has gained considerable attention because of its continuous availability in huge amount from the biodiesel production process and its capability of being a prominent chemical to synthesize value-added products. Considerable efforts have been devoted to the transformation of glycerol by various catalytic processes involving oxidation, (oxi)dehydration, reforming, etherification, esterification, hydrogenolysis, and so on [4–14].

The most significant direct application of acrolein is as an herbicide to control the growth of aquatic plants. Acrolein is also an important bulk chemical used as feedstock for production of acrylic acid, pharmaceuticals, fiber treatments, etc. The current method for manufacturing acrolein is based on oxidation of propylene or propane derived from petroleum, therefore, carbon-neutral processes for producing acrolein from glycerol will lead to lower oil consumption and reduced environmental impact.

Catalytic dehydration of glycerol to acrolein has attracted great interest. Lauriol-Garbey et al. [12] studied acid–base properties of niobium–zirconium mixed oxide catalysts for glycerol dehydration by calorimetric and catalytic measurements. Cavani et al. [13] investigated the control of selectivity in gas-phase glycerol dehydration to acrolein catalyzed by sulfated zirconia. Recently Katryniok et al. [15] overviewed the developments in the catalytic dehydration of glycerol to acrolein over the zeolite-type, heteropoly acid-type, and mixed oxide-type catalysts with respect to the observed catalytic performance as well as catalyst durability. Dubios et al. [16] reported a process for producing acrolein by gas-phase dehydration of glycerol in the presence of strongly acidic solid catalysts with Hammett acidity (H_0) between −10 and −16. Tsukuda et al. [17] investigated the production of acrolein from glycerol over silica-supported heteropoly acids. It was found that silicotungstic acid supported on mesoporous silica showed the highest activity: acrolein selectivity of 85 mol% at 548 K. They also supposed a possible reaction route. Recently, acrolein synthesis

* Corresponding author. Tel.: +86 25 83686270; fax: +86 25 83317761.
E-mail addresses: jiwj@nju.edu.cn, jiwjnju@yahoo.com (W. Ji).

http://dx.doi.org/10.1016/j.apcatb.2014.08.049
0926-3373/

from glycerol in hot-compressed water was studied by Watanabe et al. [18]. Glycerol conversion was conducted in pressurized hot water (573–673 K, 25–34.5 MPa) using both batch and flowing apparatus. Approximately acrolein selectivity of 80% was obtained at glycerol conversion of 90%. Chai et al. [19] used ZrO_2- and SiO_2-supported 12-tungstophosphoric acid catalysts and acrolein yield of 54% was obtained over the HPW/ZrO_2 catalysts. Chai et al. [20] also applied amorphous Nb_2O_5 catalyst having the highest fraction of acid sites with Hammett acidity being $8.2 \leq H_0 \leq 3.0$ for the reaction, and achieved notably high mass specific activity. Later on Xu and his co-workers extended selective glycerol dehydration over tantalum oxide and other systems [21–23]. Liu et al. [24] recently reported glycerol dehydration over the rare earth pyrophosphates and found that the pyrophosphate catalysts were active and selective toward acrolein production. They reported that catalytic activities were greatly influenced by the doped rare earth elements, and the $Nd_4(P_2O_7)_3$ catalyst exhibited 80% selectivity to acrolein at glycerol conversion of 87%. Moreover, many zeolites and modified-zeolites were tested in glycerol dehydration [25–28].

The most well-known pyrophosphate catalysts should be the vanadium pyrophosphate oxides (VPO). The VPO type catalysts have been extensively studied in the selective oxidation of butane, isobutene, propane, and ethane to the corresponding acids [29–34]. This kind of catalyst was recognized as one of the most complicated catalyst systems, and many efforts have been made to advance our understanding of catalyst nature in the partial oxidation of *n*-butane to maleic anhydride [35–43,32,44–47].

The VPO catalysts can be obtained via the dehydration of the important precursor, namely, vanadyl phosphate hemihydrate ($VOHPO_4{\cdot}0.5H_2O$). Ueda's group first studied glycerol dehydration over both a VPO precursor and an activated VPO catalyst, and found that both of them were active for the reaction [48,49]. Interestingly, the $VOHPO_4{\cdot}0.5H_2O$ precursor outperformed the activated vanadium pyrophosphate oxide catalyst, and the former also performed with maximized carbon balance (i.e., very low carbon deposition rate in reaction). It is known that preparation history (the kind of alcohol in preparation medium and the catalyst activation in particular) can have an intensive impact on the properties of VPO catalyst, including phase composition, morphology, particle size, and surface P/V ratio. It is also generally accepted that the structure of active phase and the role of V^{5+} species are the key factors for catalytic oxidations over the VPO-type catalysts [50–52]. Very recently, we found that the carefully tuned VPO catalyst comprising dominated δ-$VOPO_4$ and $(VO)_2P_2O_7$ components through an activation under an atmosphere with very low butane concentration (0.3 vol.% butane in air) was highly efficient for the aldol condensation between methyl acetate and formaldehyde to acrylic acid and its derivative [53]. In this study, we synthesized the VPO catalysts by employing different alcohols as reducing agents and solvents and the polyethylene glycol (PEG) as a specific additive in preparation medium, for glycerol dehydration to acrolein. Our previous studies confirmed that the PEG-addition in catalyst preparation can dramatically affect the physicochemical properties of VPO-type catalyst for butane selective oxidation; while the current study clearly demonstrated the role of preparation chemistry in determining the catalytic behavior of selective dehydration of glycerol to acrolein on this type of catalyst. The obtained results are informative for understanding the target reaction on the carefully identified components of VPO catalyst.

2. Experimental

2.1. Catalyst preparation

The catalyst precursors were synthesized as described previously [54]. Mixed iso-butyl and benzyl alcohols (volume ratio of 1:1) were adopted as the preparation medium. V_2O_5 was first refluxed at 140 °C for 6 h, after that PEG 6000 was introduced in suitable amount. One hour later, phosphoric acid (85%) was added drop wise to reach a P/V atomic ratio of 1.05/1.0. After another 6 h of refluxing, the suspension was filtered and the solid was washed with iso-butanol and acetone, and then dried at 100 °C in air for 24 h. The obtained precursor was denoted as $PVPO_{PEG\text{-}a}$.

Single benzyl alcohol was also used as the preparation medium. The other preparation steps are the same described above for $PVPO_{PEG\text{-}a}$ preparation. The as-synthesized precursor was denoted as $PVPO_{PEG\text{-}b}$.

Besides the precursors prepared by employing PEG additive, the reference precursor was also synthesized without using PEG, and the synthesis procedures were essentially the same except for PEG6000 introduction. The obtained precursor was denoted as $PVPO_{NPEG}$.

Before characterization and performance evaluation, all of the precursors were activated according to the following procedure. A dried precursor of 5 g was heated up from room temperature (RT) to 400 °C at a rate of 2 °C/min in a mixture of *n*-butane, N_2, and O_2 (1.5/17.2/81.3, v/v/v) with a flow rate = 20 ml min^{-1} and kept at this temperature for 15 h. The samples after activation were denoted as $VPO_{PEG\text{-}a}$, $VPO_{PEG\text{-}b}$, and VPO_{NPEG}, respectively.

2.2. Catalyst evaluation

The evaluation of catalyst activity was carried out in an upright fixed-bed quartz reactor that was 8 mm in inner diameter and 500 mm in length. The reaction was operated at atmospheric pressure. Catalyst of 0.5 g was charged into the reactor, and the space above the catalyst bed was filled with quartz chips to ensure preheating of the in-coming liquid. Before introduction of the feedstock, the sample was heated up in a flow of pure N_2 (18 ml min^{-1}) to a desired temperature at a rate of 10 °C/min and kept at this temperature for 80 min. The reaction temperature was monitored by a thermocouple inserted into the catalyst bed. After that, carrier gas was changed to a N_2—O_2 mixture (92/8, v/v). Aqueous glycerol solution (36.5 wt%) was fed at a LHSV of 4 h^{-1} by a syringe pump, and the products were collected in a cold trap after 2-h reaction. The analysis of the collected liquid was conducted using a gas chromatograph equipped with flame ionized detector (FID) and HP-FFAP capillary column (0.32 mm × 25 m), and isobutanol was adopted as an internal standard.

Glycerol conversion (%) was defined as the moles of glycerol reacted divided by the moles of glycerol fed while the product selectivity (mol%) was defined as the moles of carbon atoms in a defined product divided by the moles of carbon atoms in the reacted glycerol.

2.3. Characterization

Scanning electron microscopic (SEM) images of samples were taken on an S-4800 SEM instrument. X-ray diffraction (XRD) patterns were recorded on a Philips X'Pert MPD Pro X-ray diffractometer with graphite-monochromatized Cu K_α radiation (λ = 0.1541 nm). Raman spectra were recorded at RT on a LABRAM-HR Raman spectrometer (laser source: 514.3 nm; power: 1.0–1.5 mW). H_2-TPR was performed from RT to 800 °C at a rate of 10 °C/min in a flow of H_2/N_2 mixture (5/95, v/v) with a flow rate = 40 ml min^{-1}, and isothermally held at 800 °C until reduction was complete. TG/DTA measurement was conducted on a NETZSCH STA-449C integrated thermo-analysis instrument with the sample heated in air at a rate of 10 °C/min from RT to 700 °C. Ammonia temperature-programmed desorption (NH_3-TPD) was carried out to measure surface acidity of catalysts. Typically, 0.05 g of catalyst was heated in flowing He (30 ml min^{-1}) at 400 °C for 1 h, and

then cooled to 100 °C in the same He flow. Ammonia was subsequently introduced, and after NH_3 adsorption the sample was purged with He (30 ml min^{-1}). Finally, NH_3-TPD was carried out in He from 100 to 450 °C at a heating rate of 10 °C/min. The signal was recorded by a thermo-conductive detector. X-ray photoelectron spectroscopy (XPS) measurement was performed on a PHI5000 VersaProbe instrument with Al K_α radiation. The binding energy (BE) was calibrated against the C1s signal (284.6 eV) of contaminant carbon. Elemental surface composition was estimated on the basis of peak areas which were normalized using Wagner factors.

3. Results and discussion

3.1. SEM/BET

Fig. 1 shows the typical SEM images of the fresh VPO_{NPEG} and $VPO_{PEG\text{-}a}$, the used $VPO_{PEG\text{-}a}$, and the specifically activated $VPO_{PEG\text{-}a}$. Each sample exhibits plates and blocks in dimension of micrometers. One can see that there is no detection of the "rose-like" morphology in the fresh VPO_{NPEG} and the used $VPO_{PEG\text{-}a}$. The rudiment of "rose-like" morphology can be observed in the fresh $VPO_{PEG\text{-}a}$. The morphology of the used catalyst considerably changed, implying that the sample structure could change with time on stream of reaction. We measured the specific surface areas of three representative samples, VPO_{NPEG}, $VOP_{PEG\text{-}a}$, and $VPO_{PEG\text{-}a}$* (rose-like morphology), and the values were found to be 6.3, 17.6, and 36.9 m^2/g respectively. PEG addition in catalyst preparation increased the specific surface area of sample. Note that the amount of precursor and the flow rate employed in catalyst activation showed noticeable effect on the BET surface areas: using large amount of precursor (5 g) and low flow rate (20 ml min^{-1}) for activation resulted in small surface areas as in the cases of VPO_{NPEG} and $VOP_{PEG\text{-}a}$, while using small amount of precursor (1 g) and high flow rate (80 ml min^{-1}) for activation resulted in large surface areas as in the case of $VOP_{PEG\text{-}a}$*. Based on the results of activity evaluation (Section 3.7), however, the surface area seems not to be a determining factor for catalyst performance.

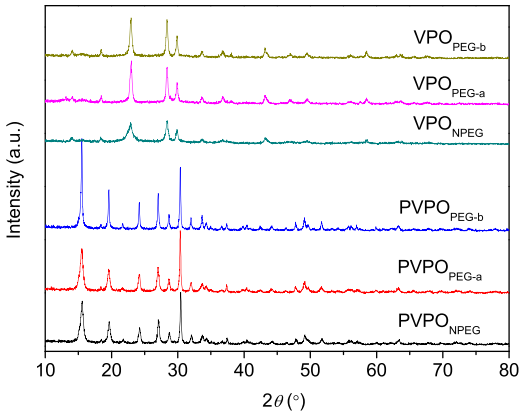

Fig. 2. XRD patterns of various PVPOs and VPOs prepared in different conditions.

3.2. XRD

Six VPO catalysts, namely, three hemihydrates ($VOHPO_4 \cdot 0.5H_2O$) and three pyrophosphates ($(VO)_2P_2O_7$) were synthesized. Their XRD patterns are shown in Fig. 2. The reflection peaks at $2\theta = 15.6°$, 19.6°, 24.2°, 27.1°, 28.7°, and 30.5° are indexed to the respective (0 0 1), (1 0 1), (2 0 0), (1 2 1), (2 0 1), and (2 2 0) plane of $VOHPO_4 \cdot 0.5H_2O$ [53]. Upon activation in *n*-butane containing atmosphere, the $VOHPO_4 \cdot 0.5H_2O$ phase underwent a topotactic dehydration to the $(VO)_2P_2O_7$ phase, as revealed by the characteristic diffraction peaks at $2\theta = 22.9°$, 28.4°, and 29.9° [55,56]. The crystallinity is somehow a measurement of the degree of crystallization which directly affects the shape and intensity of diffraction peak. A higher crystallinity generally means a larger primary particle with a higher order of atoms (ions) arrangement, corresponding

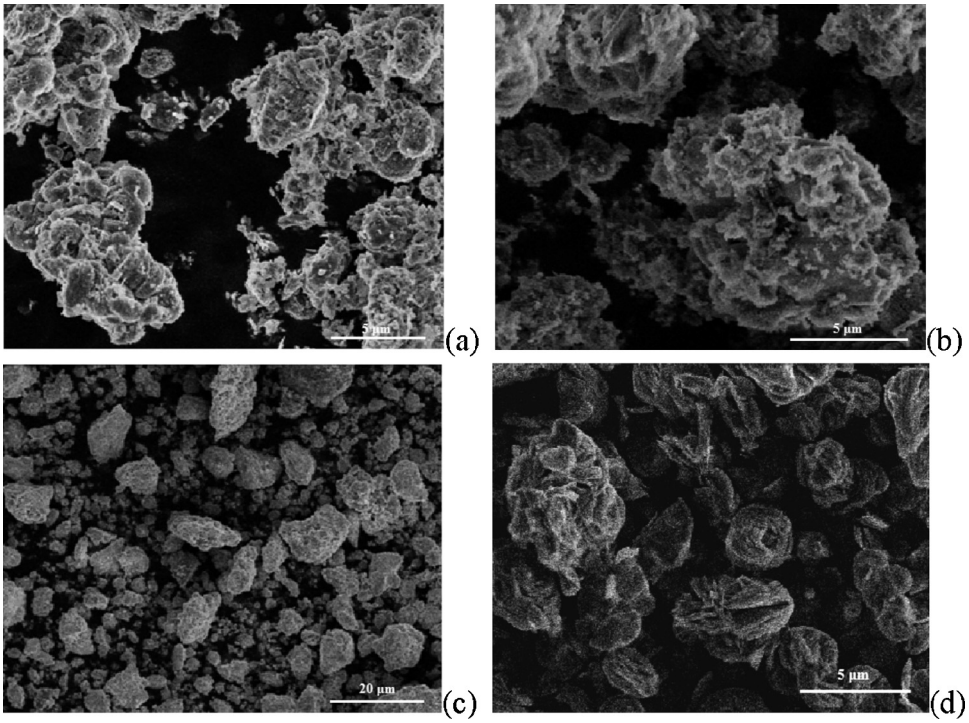

Fig. 1. SEM images of (a) VPO_{NPEG}, (b) $VPO_{PEG\text{-}a}$ (5 g $PVPO_{PEG\text{-}a}$ activated in 1.5% butane–air of 20 ml min^{-1}), (c) used $VPO_{PEG\text{-}a}$, and (d) $VPO_{PEG\text{-}a}$* (1 g $PVPO_{PEG\text{-}a}$ activated in 1.5% butane–air of 80 ml min^{-1}).

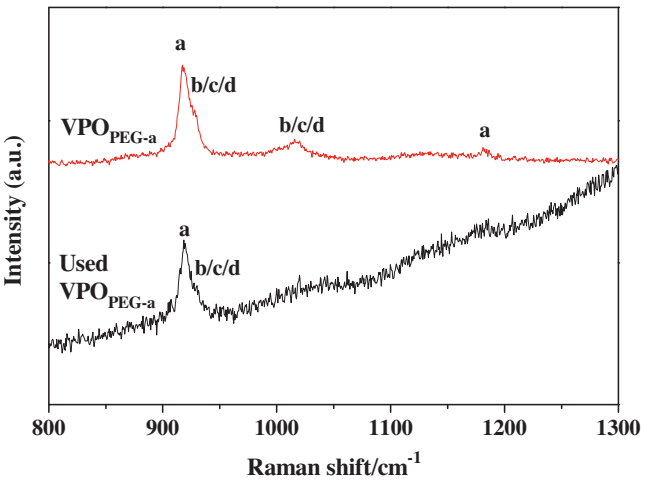

Fig. 3. Raman spectra of the fresh and used VPO_{PEG-a} catalysts. (a) $(VO)_2P_2O_7$; (b) γ-$VOPO_4$; (c) α_I-$VOPO_4$; (d) $VOPO_4{\cdot}2H_2O$.

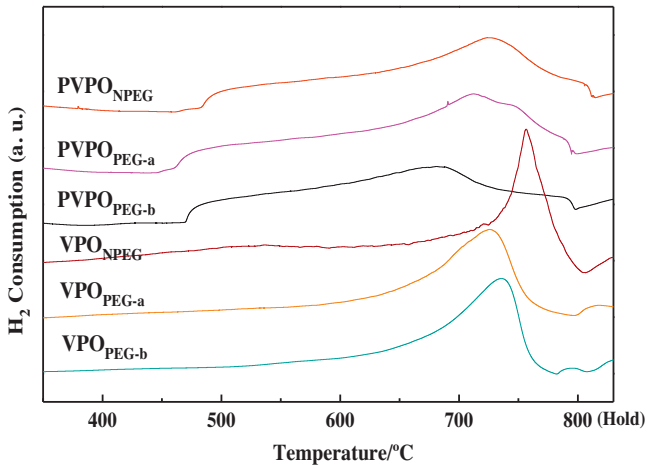

Fig. 4. H_2-TPR profiles of the various PVPOs and VPOs samples.

to sharp and intensive diffraction peaks with narrow full widths at half-maximums (FWHMs). In contrast, a lower crystallinity usually means a smaller primary particle with certain amount of structural defects, corresponding to the blunt and weak diffraction peaks with big FWHMs. Table S1 presents the maximum intensities and FWHM values of the XRD peaks at $2\theta = 15.6°$ (for the PVPOs) and 28.4° (for the VPOs), and the calculated particle sizes by the Scherrer equation. The diffraction peaks of $PVPO_{PEG-a}$ are the same as that of $PVPO_{NPEG}$, while the peak width of the former (at $2\theta = 15.6°$) somewhat increases with relatively smaller particle size, suggesting that introduction of PEG6000 in preparation should not affect the formation of the $VOHPO_4{\cdot}0.5H_2O$ phase, but show an impact on sample crystallinity [57,58]. Note that the kind of alcohol(s) in preparation media can also have an impact on the crystallinity of PVPO. For example, the crystallinity of $PVPO_{PEG-b}$ appears higher than that of $PVPO_{PEG-a}$ in terms of the values of I_{max}, FWHM, and calculated particle size. According to Table S1, PEG addition in synthesis can also enhance the crystallinity of $(VO)_2P_2O_7$ phase in the activated VPOs. The PEG addition could promote particle nucleation and favor growth of primary particles; meanwhile the generated primary particles can be covered by the PEG molecules. With a small flow rate in sample activation, the removal of residual PEG molecules from sample surfaces became slow, and the growth of $(VO)_2P_2O_7$ phase would advance gradually, resulting in the enhanced crystallinity of $(VO)_2P_2O_7$ phase in VPO_{PEG-a} and VPO_{PEG-b} (Fig. 2).

3.3. Raman

The Raman spectra of catalysts are shown in Fig. 3. The major band in the 920–930 cm^{-1} region and the small band at 1188 cm^{-1} are characteristics of the $(VO)_2P_2O_7$ species. The major band at ca. 925 cm^{-1} can be attributed to ν_{as} P—O—P in the $P_2O_7^{2-}$ unit of $(VO)_2P_2O_7$ [59,60]. The shoulder around the 925–930 cm^{-1} region together with the small band at 1020 cm^{-1} is characteristic of $VOPO_4$ species, including α_I-$VOPO_4$, γ-$VOPO_4$, and $VOPO_4{\cdot}2H_2O$ [57,61–63]. Although, the $VOPO_4$ species can be hardly distinguishable in the XRD patterns, they can be easily detected by Raman spectroscopy, especially in the surface region of catalyst.

Note that the amount of V^{5+} species reduced after reaction, since both the shoulder around 925–930 cm^{-1} and the small band at 1020 cm^{-1} decreased in their intensities. The observation implied that the content of both V^{5+} and V^{4+} species could dynamically change during the reaction course, which in turn determines the reaction behavior of catalyst.

3.4. H_2-TPR

The reduction behavior of different VPO catalysts was investigated by hydrogen temperature programmed reduction (H_2-TPR), and the results are shown in Fig. 4. There is significant difference in sample reduction between the PVPOs precursors ($VOHPO_4{\cdot}0.5H_2O$) and the activated VPOs. In the TPR profiles of the PVPOs, the baselines rose near 450 °C, while a major reduction peak appeared in the 650–750 °C range. Within the applied reduction temperature range, there is only one reduction peak centered around 650–800 °C for the activated VPOs, mainly attributable to the removal of lattice oxygen associated with the V^{4+} species.

According to the TPR profiles of the PVPOs, the V—O bonding was weakened upon PEG addition in catalyst synthesis. Note that the composition of preparation media, namely, the employed alcohol(s), showed significant effect on the reactivity of lattice oxygen of PVPOs, especially that of $PVPO_{PEG-b}$. It is worth noting that although the reactivity of lattice oxygen in the PVPOs is obviously affected by the employed alcohol(s) in preparation, there appears insignificant effect of preparation media on the V—O bond strength in the activated VPOs. However, addition of PEG in preparation can considerably weaken the V—O bonding of VPO_{PEG-a} and VPO_{PEG-b}.

It is known that the V^{5+} species in $VOPO_4$ are more easily reduced than the V^{4+} ones in $(VO)_2P_2O_7$. Therefore, a broad reduction peak of VPO_{NPEG} is attributable to the reduction of V^{5+}-containing species [51,64]. On the other hand, there is essentially no such broad reduction peak observed on VPO_{PEG-a} and VPO_{PEG-b}, which suggests that addition of PEG in preparation decrease the content of V^{5+} species in VPO_{PEG-a} and VPO_{PEG-b}. In comparison of the reduction behaviors of VPO_{PEG-a} and VPO_{PEG-b}, the main reduction peak of the former appeared at slightly lower temperature, while the initial reduction temperature of the latter was found to be lower than the former. The observations suggest that on average the V—O bonding in VPO_{PEG-a} is slightly weak than that in VPO_{PEG-b}, however, there are weakest bonded lattice oxygen atoms in VPO_{PEG-b}. Bear in mind that the observed difference in the V—O bonding strength of various samples may naturally bring about the difference in the property of surface OH groups and likewise the surface acidity of the corresponding samples.

3.5. XPS

The surface elemental composition of the fresh and used catalysts was examined by XPS technique. As shown in Table 1, the $V2p_{3/2}$ binding energies (BEs) of VPO_{NPEG}, VPO_{PEG-a} and used-VPO_{PEG-a} are around 517.0 eV, close to that (517.6 eV) reported for

Table 1
The XPS results of different VPO samples.

Catalyst	BE (eV)			Surface concentration (at %)				P/V atomic ratio
	$V2p_{3/2}$	P2p	O1s	C	O	P	V	
VPO_{NPEG}	517.1	133.7	531.4	27.4	53	11.5	8.2	1.4
VPO_{PEG-a}	517.0	133.6	531.2	12.5	62.1	15.3	10.1	1.5
VPO_{PEG-a} (used)	516.8	133.5	531.3	40.5	44.9	9.1	5.5	1.6

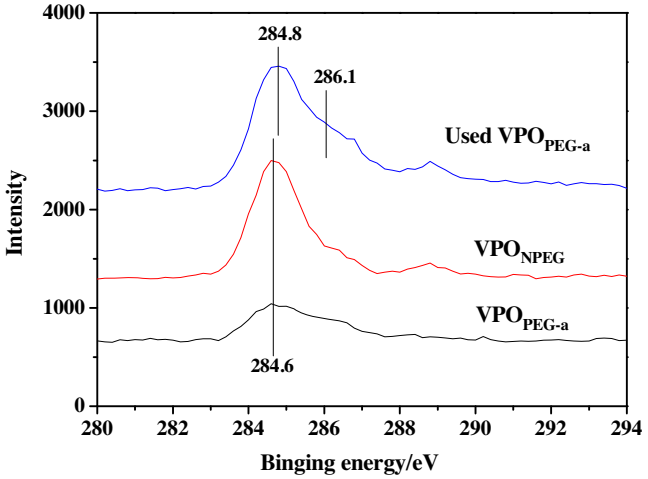

Fig. 5. C ls XPS spectra of VPO_{NPEG} and VPO_{PEG-a} as well as used VPO_{PEG-a}.

well-crystallized $(VO)_2P_2O_7$ but lower than that reported for vanadium pentoxide and V(IV) phosphate [65,66]. Hence the vanadium oxidation states of these catalysts are approximately 4+, and the VPO component is essentially in the form of $(VO)_2P_2O_7$. The $V2p_{3/2}$ BE of the used VPO_{PEG-a} is 516.8 eV, lower than that of the fresh VPO_{PEG-a}, suggesting a reduction of V^{5+} species in the used VPO_{PEG-a}. This observation is coincident with the Raman observation. Both the O1s and P2p BEs of all the catalysts are essentially similar. In addition, surface P element enrichment was observed over all of the samples. A slight "excess" of surface P element is believed to stabilize the $(VO)_2P_2O_7$ phase [64,67–69].

C1s spectra of the fresh and used catalysts are showed in Fig. 5. One can see that the C1s peak increases in intensity and shifts toward higher BE after reaction, suggesting the deposition of carbonaceous species during the reaction. From Table 1, one can see that the relative surface V, P, and O concentrations also decrease as a result of surface carbonaceous deposit. Interestingly, the relative surface C coverage of the fresh VPO_{PEG-a} appears lower than that of the fresh VPO_{NPEG}, which implies a higher fraction of active surface available for reaction.

Table 2
Relative amount of V^{5+} and V^{4+} derived from the curve fitting analysis of the $V2p_{3/2}$ peaks.

Catalyst	VPO_{NPEG}	VPO_{PEG-a}	Used VPO_{PEG-a}	VPO_{PEG-b}*[a]
V^{5+} (at %)	2.0	2.0	0.8	3.6
V^{4+} (at %)	6.2	8.1	4.7	5.8
V^{5+}/V^{4+}	0.32	0.25	0.17	0.62

[a] $PVPO_{PEG-b}$* was activated in the mixture of 0.3% *n*-butane/air (v/v).

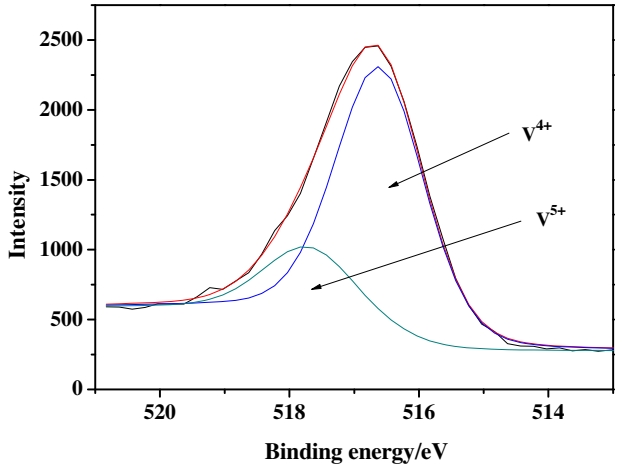

Fig. 6. Curve fitting analysis of the $V2p_{3/2}$ peak of VPO_{PEG-a}.

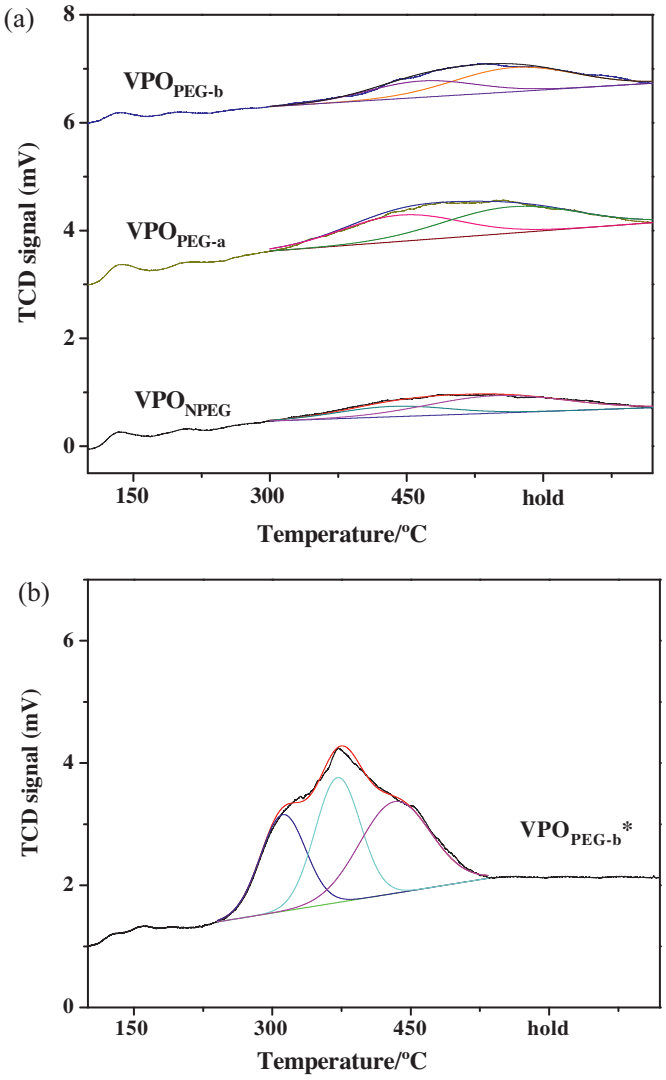

Fig. 7. (a) NH_3-TPD profiles of VPO_{PEG-a}, VPO_{PEG-b}, and VPO_{NPEG} with different quantity of surface V^{5+} and V^{4+} species and (b) NH_3-TPD profile of VPO_{PEG-b}* with the highest fraction of surface V^{5+} species.

With deconvolution analysis of the V2p$_{3/2}$ spectra, one can roughly estimate the surface V^{5+} and V^{4+} proportions (Fig. 6), and the data are included in Table 2. Although an accurate comparison among the relative surface V^{5+} and V^{4+} concentrations of three VPO catalysts could be ambitious, roughly speaking, the surface V^{4+} concentration was found to be the largest over the fresh $VPO_{PEG\text{-}a}$, and it reduced notably over the used $VPO_{PEG\text{-}a}$. In addition, there is obvious difference in the surface V^{5+}/V^{4+} ratios of three VPO catalysts. Among the fresh VPO_{NPEG}, the fresh $VPO_{PEG\text{-}a}$, and the used $VPO_{PEG\text{-}a}$, the first one has the highest V^{5+}/V^{4+} ratio, the second one shows a medium value, while the last one the lowest. Note that the $PVPO_{PEG\text{-}b}$* sample which was activated in the mixture of 0.3% *n*-butane/air (v/v) indicates even a much higher V^{5+}/V^{4+} ratio. As revealed later in activity evaluation, the most active catalyst $VPO_{PEG\text{-}a}$ has the balanced V^{5+}/V^{4+} ratio. The results also explained the declined catalyst activity with time on stream (see Section 3.7.3), since the surface V^{5+}/V^{4+} ratio continuously decreases during the reaction, and such change in surface V^{5+}/V^{4+} ratio would particularly affect the selectivity to acrolein.

3.6. NH_3-TPD

It is known that the glycerol dehydration can be catalyzed by acids and bases. Certain correlations between the acidity/basicity of catalysts and the catalyst performances (conversion and selectivity) have been established over a few systems [15]. According to our NH_3-TPD study (Fig. 7), the catalysts of $VPO_{PEG\text{-}a}$, $VPO_{PEG\text{-}b}$, and VPO_{NPEG} showed both weak (corresponding to the NH_3 desorption peaks in the temperature range from 80 to 230 °C) and medium to strong acid sites (corresponding to the NH_3 desorption peaks beyond 300 °C). The deconvolution of the broad NH_3 TPD profiles in the high temperature range was conducted (Fig. 7a). The results showed similar trend and there were essentially two peaks separated out. According to the summed peak areas, the overall acid site density with medium strong acid strength in the three samples showed the following order: $VPO_{PEG\text{-}a} > VPO_{PEG\text{-}b} > VPO_{NPEG}$. On $VPO_{PEG\text{-}a}$, the two fitted peaks are nearly equal in peak area, while on $VPO_{PEG\text{-}b}$ and VPO_{NPEG}, there appear small peaks associated with relatively low desorption temperatures. Clearly, employing the mixed iso-butyl and benzyl alcohols would maximize Brønsted surface acidity of catalyst, which was also supported by the IR bands of NH_3 adsorption (ca. 1430 cm^{-1}) on $VPO_{PEG\text{-}a}$ and $VPO_{PEG\text{-}b}$ (Fig. S1, Supplementary Material). Interestingly, in $VPO_{PEG\text{-}b}$* which was obtained by activating $PVPO_{PEG\text{-}b}$ in an atmosphere with a lower butane concentration (0.3% butane–air), there was notable enhancement in acid site density but certain reduction in acid strength (Fig. 7b). The observed change in surface acid property was resulted from the change in sample constitution as revealed by Raman investigation [53]: a large fraction of the δ-$VOPO_4$ entity together with the $(VO)_2P_2O_7$ one. This is additional example showing a close correlation between the V^{5+}/V^{4+} ratio and the acid density/strength on the VPO-based catalyst. In line with the results of activity evaluation on $VPO_{PEG\text{-}b}$* (see below), one can infer that besides its oxidation ability, the acid site density of certain strength may also play a role in determining the product distribution on this catalyst. We also investigated the surface basicity of the VPO catalysts (Fig. S2, Supplementary Material) by means of the CO_2-TPD technique, the results indicated, however, that the surface basicity of the current VPO catalysts was little affected by changing the synthetic parameters adopted in this study.

3.7. Catalytic performance

Catalytic activities over various VPO catalysts are summarized in Table 3. One can see that catalytic activities of the VPOs are highly dependent on the following factors: (1) generally speaking, the catalyst precursors (PVPOs) are less active than the corresponding activated catalysts (VPOs) in the current study, which is different from the observation made by Wang et al. [48]. Among the three precursors, addition of PEG and use of different alcohol(s) in preparation showed certain effects on the activities of PVPOs. In light of the acrolein yields, the effect of PEG addition on the performances of PVPOs is insignificant; on the other hand, the PEG addition can notably enhance acrylic acid formation. This is understandable because the reactivity of the lattice oxygen associated with V^{5+} and V^{4+} species in $PVPO_{PEG\text{-}a}$ and $PVPO_{PEG\text{-}b}$ is enhanced

Table 3
Catalytic activities obtained over various VPO catalysts.[a]

Catalyst	Glycerol conversion (%)	Yield of products (mol%)				Acrolein selectivity (mol%)	Acrolein formation rate (mmol g_{cat}^{-1} h^{-1})
		Acrolein	Acrylic acid	Acetic acid	Others[b]		
$PVPO_{NPEG}$	72.0	23.3	9.9	1.8	32.4	32.4	4.0
$PVPO_{PEG\text{-}a}$	93.3	18.8	16.7	3.7	54.1	20.2	3.2
$PVPO_{PEG\text{-}b}$	88.7	23.3	16.1	2.8	46.5	26.3	4.0
VPO_{NPEG}	97.7	27.8	13.9	10.1	45.9	28.5	4.8
$VPO_{PEG\text{-}a}$	100.0	62.3	0.0	2.7	35.0	62.3	10.7
$VPO_{PEG\text{-}b}$	100.0	51.9	0.9	10.1	37.1	51.9	8.9
$VPO_{PEG\text{-}a}$[c]	100.0	70.1	0.0	1.3	28.6	70.1	12.0
$VPO_{PEG\text{-}a}$[d]	99.1	60.8	1.7	1.8	34.8	61.4	10.3
$VPO_{PEG\text{-}b}$*[e]	100.0	25.3	7.8	6.8	60.1	25.3	4.3
$VPO_{PEG\text{-}a}$[f]	97.4	64.2	2.9	1.8	28.5	65.9	11.0
$VPO_{PEG\text{-}a}$[g]	100.0	65.2	0.0	3.4	31.4	65.2	11.2
$VPO_{PEG\text{-}b}$[h]	100.0	63.2	0.0	4.5	32.3	63.2	10.8

[a] Catalyst of 0.5 g was positioned under quartz chips (40–60 mesh). Reaction temperature = 300 °C. The aqueous glycerol solution (36.5 wt.%) was fed at a liquid hourly space velocity (LHSV) of 4 h^{-1}. A nitrogen–air mixture was employed as a carrier (30 ml min^{-1}), in which the oxygen content is 8 vol.%. The collected sample was analyzed after 2-h reaction.

[b] On PVPOs, the fraction of hydroxyacetone and acetaldehyde is 1–1.5%, the fraction of carbonaceous species is <2.5%, and the fraction of heavy and unknown compounds is 17–28%, while that of CO_x is approximately 16–23%. On VPO_{NPEG}, the fraction of hydroxyacetone and acetaldehyde is ca. 1%, the fraction of carbonaceous species is 2%, and the fraction of heavy and unknown compounds is 21%, while that of CO_x is around 23%. On $VPO_{PEG\text{-}a}$ and $VPO_{PEG\text{-}b}$, the fraction of hydroxyacetone and acetaldehyde is <1%, the fraction of carbonaceous species is <2%, the fraction of heavy and unknown compounds is 8–10%, while that of CO_x is around 22–26%.

[c] Reaction temperature = 320 °C. No detectable heavy and unknown compounds except for hydroxyacetone and acetaldehyde of <1%, carbonaceous species of 1.8%, and CO_x of 25.8%.

[d] Reaction temperature = 290 °C.

[e] $PVPO_{PEG\text{-}b}$* was activated in the mixture of 0.3% *n*-butane/air (v/v), reaction temperature = 300 °C. There are heavy and unknown compounds of 34%.

[f] Reaction temperature = 320 °C, oxygen concentration (vol.%) = 5.

[g] $PVPO_{PEG\text{-}a}$ of 1 g was activated in the mixture of *n*-butane/N_2/O_2 (1.5/17.2/81.3, v/v/v, 80 ml min^{-1}), reaction temperature = 320 °C.

[h] $PVPO_{PEG\text{-}b}$ of 1 g was activated in the mixture of *n*-butane/N_2/O_2 (1.5/17.2/81.3, v/v/v, 80 ml min^{-1}), reaction temperature = 320 °C.

according to the H_2-TPR results (Fig. 4), which favors the oxygen insertion into the C—H bond to generate carboxyl group (acrylic acid). Moreover, employing benzyl alcohol in precursor synthesis ($PVPO_{PEG\text{-}b}$) showed a positive effect on acrolein production. (2) Among the three activated VPO catalysts, the effect of PEG addition is dramatic: the acrolein yield obtained on VPO_{NPEN} is only 27.8 mol%, while that achieved on $VPO_{PEG\text{-}a}$ and $VPO_{PEG\text{-}b}$ is 62.3% and 51.9%, respectively. Interestingly, there is an opposite effect of employed alcohol(s) on the performances of activated VPOs: $VPO_{PEG\text{-}a}$ synthesized using mixed iso-butanol and benzyl alcohol is superior to $VPO_{PEG\text{-}b}$ synthesized using single benzyl alcohol. According to Table 3, on PVPOs as well as VPO_{NPEG}, more acrolein seems to be oxidized to acrylic acid and acetic acid but limited to CO_x, meanwhile notable fraction of glycerol is converted into the heavy and unknown compounds. On $VPO_{PEG\text{-}a}$ and $VPO_{PEG\text{-}b}$, less amount of acrolein is oxidized to acrylic acid and acetic acid, and equally important feature is that only small fraction of glycerol is converted into the heavy and unknown compounds. Specifically, when operated at 320 °C, $VPO_{PEG\text{-}a}$ showed no detectable heavy and unknown compounds except for hydroxyacetone and acetaldehyde of <1%, carbonaceous species of 1.8%, and CO_x of 25.8%. In the case of $VPO_{PEG\text{-}b}{}^*$ which comprises higher content of V^{5+} species (Table 3), once again, large portion of acrolein is oxidized to acrylic acid and acetic acid, and particularly, great amount of glycerol is converted into the heavy and unknown compounds (34%).

According to the characterizations of Raman, XPS, and NH_3-TPD, there are two facts revealed: the preparation chemistry involving PEG introduction, change of preparation medium and activation manner can have significant impact on: (i) the ratio of V^{5+} species (in $VOPO_4$) to V^{4+} species (in $(VO)_2P_2O_7$) (Table 2) which determines the oxidation ability of catalyst and further influences the product distribution of acrolein, acrylic acid, acetic acid, as well as CO_x (Table 3); and (ii) the surface acid property (Fig. 7) which determines the efficiency of glycerol dehydration and also likely the production distribution (Table 3). The characterization results also demonstrated that the V^{5+}/V^{4+} ratio of the VPO-based catalysts affected not only the acid site density but also the acid strength (Fig. 7a and b), which in turn had an impact on the reaction pathways of glycerol dehydration and possible condensations as suggested by Chieregato et al. [11] and observed by us [53]. As clarified by previous studies [2], the enhancement in surface Brønsted acidity of certain strength favored the reaction pathway of glycerol dehydration to acrolein; on the other hand, the increasing surface V^{5+} fraction in the current catalyst system could favor the consecutive deep oxidation of dehydrated product – acrolein to acrylic acid (as a result of oxygen insertion), to acetic acid (as a result of C—C bond cleavage), and eventually to CO_x (as a result of complete oxidation/combustion). Therefore, a well-balanced V^{5+}/V^{4+} ratio of a catalyst such as in the case of $VPO_{PEG\text{-}a}$, corresponds to appropriate surface acidity as well as oxidation ability, ensuring efficient dehydration of glycerol yet not too significant deep oxidation and other side-reaction of the desired products.

Considering the high feed rate of glycerol, the acrolein formation rate of 12.0 mmol $g_{cat}{}^{-1}$ h^{-1} was achieved on $VPO_{PEG\text{-}a}$. In addition, if small amount (1 g) of $PVPO_{PEG}$ was activated in a 1.5% butane–air flow of higher flow rate (80 ml min^{-1}), the corresponding VPO catalysts also performed well for acrolein generation. It is worth noting that the derived VPOs in these cases are well-crystallized, with the typical "rose-like" morphology (Fig. 1D). In terms of the above discussion, one can infer that the preparation chemistry (particularly the PEG addition) can significantly modify the nature of VPO type catalysts and enhance the selective acrolein formation accordingly.

3.7.1. *Effect of reaction temperature and O_2 content in carrier*

The yields of acrolein and acrylic/acetic acids and conversion of glycerol at different temperatures are showed in Fig. 8a. One

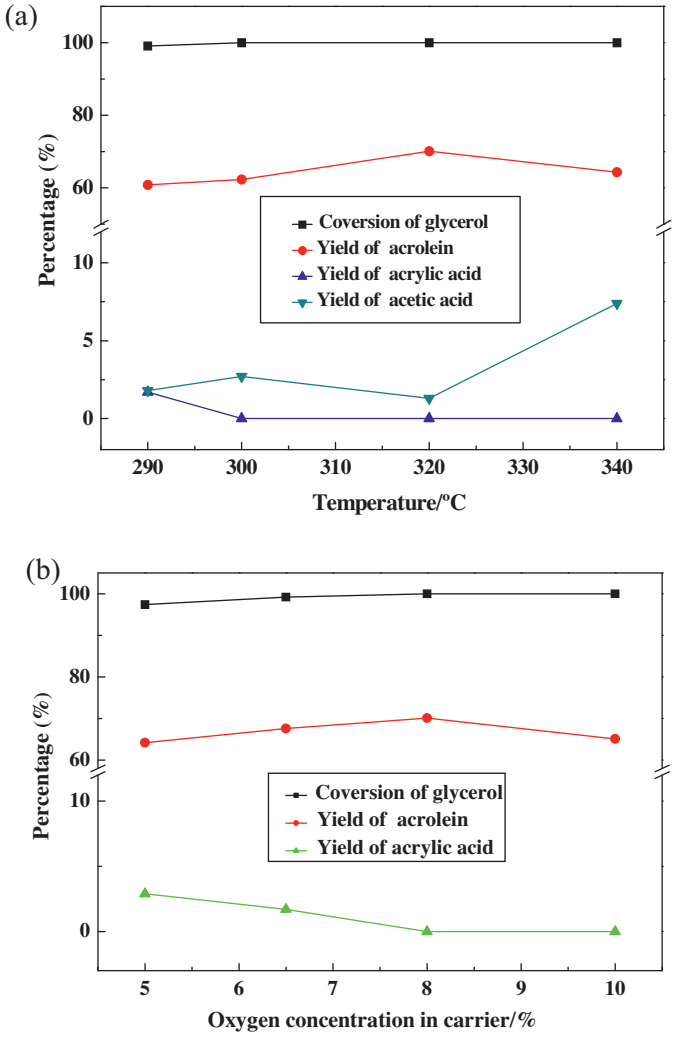

Fig. 8. (a) Temperature dependence of catalytic performance of $VPO_{PEG\text{-}a}$ (glycerol concentration = 36.5 wt.%, and oxygen concentration = 8 vol.%). (b) Effect of oxygen concentration on catalytic performance of $VPO_{PEG\text{-}a}$ (glycerol concentration = 36.5 wt.%, and reaction temperature = 320 °C).

can see that complete glycerol conversion can be achieved within the 300–340 °C range. The highest acrolein yield was obtained at 320 °C. With further rise in reaction temperature, the acrolein selectivity declined again. It is meaningful to see the change in selectivity of acrolein as well as acrylic acid at lower conversion of glycerol, and the reaction was once operated at 270 °C. However, some condensation of glycerol was observed, and it might result from a cold spot in the reaction setup. To avoid such an issue, the reaction was tested at a temperature as low as 290 °C. The data indicated that glycerol conversion slightly decreased (99.1%), meanwhile acrolein yield also slightly declined to 60.8% with acrylic acid yield of 1.7%. It seems that lowing reaction temperature could enhance acrylic acid selectivity at the expense of acrolein one.

Effect of oxygen concentration in the carrier gas on catalytic performance is showed in Fig. 8b. Glycerol conversion slightly increases with increasing oxygen concentration (from 5 to 8 vol.%). Complete glycerol conversion maintained at higher oxygen concentrations. The highest acrolein yield was obtained at oxygen concentration of 8 vol.%. Small amount of acrylic acid was produced at the oxygen concentration of 5–8 vol.%; on the contrary, acetic acid other than acrylic acid was produced at the oxygen concentration of 8–10% (not shown).

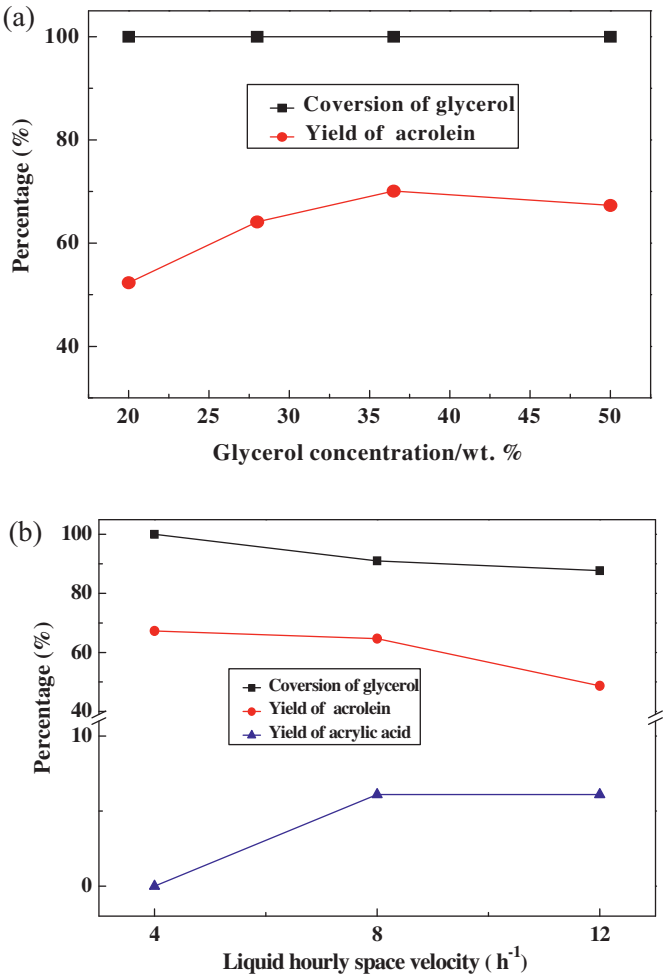

Fig. 9. (a) Effect of glycerol concentration on catalytic performance of $VPO_{PEG\text{-}a}$ (reaction temperature = 320 °C, and oxygen concentration = 8 vol.%). (b) Effect of LHSV on catalytic performance of $VPO_{PEG\text{-}a}$. Glycerol concentration = 50 wt.% (reaction temperature = 320 °C, and oxygen concentration = 8 vol.%).

The results suggest that acrolein can be oxidized to acrylic acid at relatively lower oxygen concentration; while the C—C bond cleavage of acrylic acid can occur at higher oxygen concentration, leading to the generation of acetic acid.

3.7.2. *Effect of glycerol concentration in solution and liquid hourly space velocity*

According to Fig. 9a, complete glycerol conversion can be obtained employing an aqueous glycerol solution of 20–50% concentration at 320 °C. The highest acrolein yield (70.1%) was obtained at a glycerol concentration of 36.5%. Only trace of acrylic acid was detected in the whole glycerol concentration range tested. However, certain amount of acetic acid was detected when using the glycerol concentration of 20–30%. Note that even the glycerol concentration reaches 50%, the level of acrolein yield was still sufficiently high (approximately 66%), giving the formation rate of 16.4 mmol g_{cat}^{-1} h^{-1}.

Effect of LHSV of aqueous glycerol solution (50 wt%) on reaction performance was investigated (Fig. 9b). Within the range of LHSV studied, acrolein is the major product with small fraction of acetaldehyde. With increasing LHSV of 4–12 h^{-1}, the glycerol conversion decreases from 100% to 88%. The $VPO_{PEG\text{-}a}$ catalyst can handle a heavy loading of reaction feed, for instance, a notably higher LHSV of 12 h^{-1}, and still retain a reasonable acrolein yield (~48 mol%), giving significantly high acrolein formation rate up to

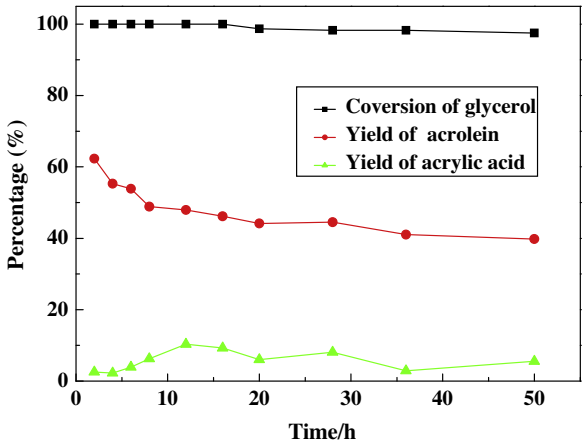

Fig. 10. Stability of $VPO_{PEG\text{-}a}$ at 300 °C for 50 h. Glycerol concentration = 36.5 wt.%, and oxygen concentration = 8 vol.%.

35.3 mmol g_{cat}^{-1} h^{-1}. To the best of our knowledge, it is the highest value known to date for glycerol dehydration to acrolein. With increasing LHSV, certain amount of acrylic acid is produced. This is understandable since a higher glycerol/oxygen ratio would reduce the possibility of C—C bond breakage, which favors acrylic acid meanwhile inhibits acetic acid formation.

3.7.3. *Stability of $VPO_{PEG\text{-}a}$*

Glycerol conversion and acrolein/acrylic acid yields change with time on stream (TOS) was investigated over $VPO_{PEG\text{-}a}$ at 300 °C (Fig. 10). Although glycerol conversion dropped very slowly, acrolein yield declined steadily in the first 10 h, it kept more stable after 20 h reaction, showing the acrolein yield of ca. 40 mol%. Acrylic acid yield changed insignificantly within a TOS of 50 h. The TG-DTA investigations were conducted over the used $VPO_{PEG\text{-}a}$ sample (Fig. S3, Supplementary Material). The TG profile together with the DTA one clearly suggests the weight loss up to 450 °C is due to the elimination of deposited surface carbon. Based on the TG studies and the normalization with respect to a fresh catalyst, an initial carbon deposition rate on the used catalyst was approximately 11.3 mg g_{cat}^{-1} h^{-1}, corresponding to a fraction of glycerol input of 1.8% by weight.

4. Conclusions

In the present study, we synthesized different VPO catalysts by changing the preparation conditions, particularly the introduction of PEG additive in preparation media, to modify catalyst nature and to figure out the key factors that determine catalyst performance for glycerol dehydration. Based on the systematic characterization and activity evaluation, the following conclusions were made:

(1) In fabrication of VPO catalyst, the mixed isobutanol and benzyl alcohol showed better outcome than the single benzyl alcohol. Introduction of PEG additive to preparation media can significantly enhance the so-derived VPO catalyst performance. Acrolein yield of 70.1 mol% can be obtained over $VPO_{PEG\text{-}a}$ under the following conditions: an aqueous glycerol solution feed (36.5 wt%) with LHSV = 4 h^{-1} and reaction temperature of 320 °C. The $VPO_{PEG\text{-}a}$ catalyst can handle heavy loading of reaction feed, for instance, a concentrated glycerol solution (50.0 wt%) or a notably higher LHSV of 12 h^{-1}, and still retain reasonable acrolein yields (45–65 mol%), giving significantly high acrolein formation rates (16.4–35.3 mmol g_{cat}^{-1} h^{-1}).
(2) Within a TOS of 50 h at 300 °C, glycerol conversion declined slowly. Acrolein yield decreased steadily in the first 10 h, and

kept more stable after 20 h reaction, maintaining the acrolein yield of ca. 40%.

(3) The type of alcohol and addition of PEG in preparation media showed remarkable impact on the crystallinity and morphology of PVPOs and VPOs, the V—O bonding, and the surface V^{5+}/V^{4+} ratio in various catalysts. Raman spectroscopic study indicates the presence of V^{5+} specimen and the change of its content during the reaction running. XPS study revealed significant decrease in the V^{5+}/V^{4+} ratio and the deposition of surface carbon species after reaction, which may account for the observed catalyst deactivation. Well-balanced surface V^{5+}/V^{4+} ratio and appropriate density of medium strong acid sites in $VPO_{PEG\text{-}a}$ are found to be critical to accomplish superior activity.

Acknowledgments

We thank the financial support from MSTC (2013AA031703), NSFC (21173118), NSFJS (BK2011439), and MOE (20110091110023).

Appendix A. Supplementary data

Supplementary data associated with this article can be found, in the online version, at http://dx.doi.org/10.1016/j.apcatb.2014.08.049.

References

[1] A. Corma, S. Iborra, A. Velty, Chem. Rev. 107 (2007) 2411–2502.
[2] J.N. Chheda, G.W. Huber, J.A. Dumesic, Angew. Chem. Int. Ed. 46 (2007) 7164–7183.
[3] G.W. Huber, S. Iborra, A. Corma, Chem. Rev. 106 (2006) 4044–4098.
[4] A. Behr, J. Eilting, K. Irawadi, J. Leschinski, F. Lindner, Green Chem. 10 (2008) 13–30.
[5] D. Ten Jeroen, U. Hanefeld, ChemSusChem 4 (2011) 1017–1034.
[6] Y. Nakagawa, K. Tomishige, Catal. Sci. Technol. 1 (2011) 179–190.
[7] C.H. Zhou, J.N. Beltramini, Y.X. Fan, G.Q. Lu, Chem. Soc. Rev. 37 (2008) 527–549.
[8] M. Pagliaro, R. Ciriminna, H. Kimura, M. Rossi, C. Della Pina, Angew. Chem. Int. Ed. 46 (2007) 4434–4440.
[9] J.A. Posada, L.E. Rincón, C.A. Cardona, Bioresour. Technol. 111 (2012) 282–293.
[10] S.H. Zhu, Y.L. Zhu, S.L. Hao, H.Y. Zheng, T. Mo, Y.W. Li, Green Chem. 14 (2012) 2607–2616.
[11] A. Chieregato, M.D. Soriano, F. Basile, G. Liosi, S. Zamora, P. Concepción, F. Cavani, J.M. López Nieto, Appl. Catal. B: Environ. 150–151 (2014) 37–46.
[12] P. Lauriol-Garbey, G. Postole, S. Loridant, A. Auroux, V. Belliere-Baca, P. Rey, J.M.M. Millet, Appl. Catal. B: Environ. 106 (2011) 94–102.
[13] F. Cavani, S. Guidetti, L. Marinelli, M. Piccinini, E. Ghedini, M. Signoretto, Appl. Catal. B: Environ. 100 (2010) 197–204.
[14] Z.L. Yuan, L.N. Wang, J.H. Wang, S.X. Xia, P. Chen, Z.Y. Hou, X.M. Zheng, Appl. Catal. B: Environ. 101 (2011) 431–440.
[15] B. Katryniok, S. Paul, F. Dumeignil, ACS Catal. 3 (2013) 1819–1834.
[16] J.L. Dubois, C. Duquenne, W. Hoelderich, J. Kervennal, World Organization Patent 2006087084 (2006).
[17] E. Tsukuda, S. Sato, R. Takahashi, T. Sodesawa, Catal. Commun. 8 (2007) 1349–1353.
[18] M. Watanabe, T. Iida, Y. Aizawa, T.M. Aida, H. Inomata, Bioresour. Technol. 98 (2007) 1285–1290.
[19] S.H. Chai, H.P. Wang, Y. Liang, B.Q. Xu, Green Chem. 10 (2008) 1087–1093.
[20] S.H. Chai, H.P. Wang, Y. Liang, B.Q. Xu, J. Catal. 250 (2007) 342–349.
[21] L.T. Tao, B. Yan, Y. Liang, B.Q. Xu, Green Chem. 15 (2013) 696–705.
[22] S.H. Chai, H.P. Wang, Y. Liang, B.Q. Xu, Appl. Catal. A 353 (2009) 213–222.
[23] S.H. Chai, L.Z. Tao, B. Yan, J.C. Vedrine, B.Q. Xu, RSC Adv. 4 (2014) 4619–4630.
[24] Q.B. Liu, Z. Zhang, Y. Du, J. Li, X.G. Yang, Catal. Lett. 127 (2009) 419–428.
[25] C.J. Zhou, C.J. Huang, W.G. Zhang, H.S. Zhai, H.L. Wu, Z.S. Chao, Stud. Surf. Sci. Catal. 165 (2007) 527–530.
[26] C.J. Jia, Y. Liu, W. Schmidt, A.H. Lu, F. Schüth, J. Catal. 269 (2010) 71–79.
[27] Y.T. Kim, K.D. Jung, E.D. Park, Micropor. Mesopor. Mater. 131 (2010) 28–36.
[28] A.S. Oliveira, S.J.S. Vasconcelos, J.R. Sousa, F.F. Sousa, J.M. Filho, A.C. Oliverira, Chem. Eng. J. 168 (2011) 765–774.
[29] G.J. Hutchings, J. Mater. Chem. 19 (2009) 1222–1235.
[30] G.S. Patience, R.E. Bockrath, J.D. Sullivan, H.S. Horowitz, Ind. Eng. Chem. Res. 46 (2007) 4374–4381.
[31] G. Centi, J.L. Nieto, D. Pinelli, F. Trifiro, Ind. Eng. Chem. Res. 28 (1989) 400–406.
[32] V.V. Guliants, S.A. Holmes, J.B. Benziger, P. Heaney, D. Yates, I.E. Wachs, J. Mol. Catal. A 172 (2001) 265–276.
[33] N. Ballarini, F. Cavani, C. Cortelli, S. Ligi, F. Pierelli, F. Trifiro, C. Fumagalli, G. Mazzoni, T. Monti, Top. Catal. 38 (2006) 147–156.
[34] Q. Jiang, J. Zhao, X.K. Li, W.J. Ji, Z.B. Zhang, C.T. Au, Appl. Catal. A 341 (2008) 70–76.
[35] G. Centi, F. Trifirò, J.R. Ebner, V.M. Franchetti, Chem. Rev. 88 (1988) 55–80.
[36] J.R. Ebner, M.R. Thompson, Catal. Today 16 (1993) 51–60.
[37] R. Nilsson, T. Lindblad, A. Andersson, J. Catal. 148 (1994) 501–513.
[38] C.J. Kiely, A. Burrows, G.J. Hutchings, K.E. Bere, J.C. Volta, A. Tuel, M. Abon, Faraday Discuss. 105 (1996) 103–118.
[39] S. Albonetti, F. Cavani, F. Trifiro, Catal. Rev. Sci. Eng. 38 (1996) 413–438.
[40] K.E. Birkeland, S.M. Babitz, G.K. Bethke, H.H. Kung, G.W. Coulston, S.R. Bare, J. Phys. Chem. B 101 (1997) 6895–6902.
[41] G.W. Coulston, S.R. Bare, H. Kung, K. Birkeland, G.K. Bethke, R. Harlow, N. Herron, P.L. Lee, Science 275 (1997) 191–193.
[42] J.-M. Herrmann, P. Vernoux, K.E. Béré, M. Abon, J. Catal. 167 (1997) 106–117.
[43] L.M. Cornaglia, C.R. Carrara, J.O. Petunchi, E.A. Lombardo, Catal. Today 57 (2000) 313–322.
[44] G.J. Hutchings, J.A. Lopez- Sanchez, J.K. Bartley, J.M. Webster, A. Burrows, C.J. Kiely, A.F. Carley, C. Rhodes, M. Havecker, A. Knop-Gericke, R.W. Mayer, R. Schlogl, J.C. Volta, M. Poliakoff, J. Catal. 208 (2002) 197–210.
[45] N. Hiyoshi, N. Yamamoto, N. Ryumon, Y. Kamiya, T. Okuhara, J. Catal. 221 (2004) 225–233.
[46] M.J. Lorences, G.S. Patience, F.V. Díez, J. Coca, Appl. Catal. A 263 (2004) 193–202.
[47] M. Conte, G. Budroni, J.K. Bartley, S.H. Taylor, A.F. Carley, A. Schmidt, D.M. Murphy, F. Girgsdies, T. Ressler, R. Schlögl, G.J. Hutchings, Science 313 (2006) 1270–1273.
[48] F. Wang, J.L. Dubois, W. Ueda, J. Catal. 268 (2009) 260–267.
[49] F. Wang, J.L. Dubois, W. Ueda, Appl. Catal. A 376 (2010) 25–32.
[50] C.Y. Xiao, X. Chen, Z.Y. Wang, W.J. Ji, Y. Chen, C.T. Au, Catal. Today 93–95 (2004) 223–228.
[51] G.J. Hutchings, C.A. Dismasting, R. Oliver, J.C. Volta, Nature 368 (1994) 41–45.
[52] X.K. Li, W.J. Ji, J. Zhao, Z.B. Zhang, C.T. Au, J. Catal. 238 (2006) 232–241.
[53] X.Z. Feng, B. Sun, Y. Yao, Q. Su, W.J. Ji, C.T. Au, J. Catal. 314 (2014) 132–141.
[54] W.J. Ji, L.J. Xu, X.S. Wang, Z. Hu, Q.J. Yan, Y. Chen, Catal. Today 74 (2002) 101–110.
[55] A.M.D. Farias, W.A. Gonzalez, P.G.P. Oliveira, J.G. Eon, J.M. Herrmann, M. Aouine, S. Loridant, J.C. Volta, J. Catal. 208 (2002) 238–246.
[56] E. Bordes, P. Courtine, J. Catal. 57 (1979) 236–252.
[57] V.V. Guliants, J.B. Benziger, S. Sundaresan, I.E. Wachs, J.M. Jehng, J.E. Roberts, Catal. Today 28 (1996) 275–295.
[58] G. Busca, F. Cavani, G. Centi, F. Trifirò, J. Catal. 99 (1986) 400–414.
[59] S. Irusta, A. Boix, B. Pierini, C. Caspani, J. Petunchi, J. Catal. 187 (1999) 298–310.
[60] M.T. Sananés-Schulz, F. Ben Abdelouahab, G.J. Hutchings, J.C. Volta, J. Catal. 163 (1996) 346–353.
[61] R.M. Feng, X.J. Yang, W.J. Ji, Y. Chen, C.T. Au, J. Catal. 246 (2007) 166–176.
[62] T.P. Moser, G.L. Schrader, J. Catal. 92 (1985) 216–231.
[63] F.B. Abdelouahab, R. Oliver, N. Guillaume, F. Lefebvre, J.C. Volta, J. Catal. 134 (1992) 151–167.
[64] X.S. Wang, L.J. Xu, X. Chen, W.J. Ji, Q.J. Yan, Y. Chen, J. Mol. Catal. A: Chem. 206 (2003) 261–268.
[65] B.K. Hodnett, Catal. Rev. Sci. Eng. 27 (1985) 373–424.
[66] V.I. Bukhtiyarov, Catal. Today 56 (2000) 403–413.
[67] G. Landi, L. Lisi, J.C. Volta, Catal. Today 91–92 (2004) 275–279.
[68] R.A. Overbeek, A.R.C.J. Pekelharing, A.J. van Dillen, J.W. Geus, Appl. Catal. A 135 (1996) 231–248.
[69] R.A. Overbeek, P.A. Warringa, M.J.D. Crombag, L.M. Visser, A.J. van Dillen, J.W. Geus, Appl. Catal. A 135 (1996) 209–230.